Computer Assisted Mechanics and Engineering Sciences, 5: 345–359, 1998.

Vibrational power flow in beam-plate structures Part I: Basic theory

Chuijie Yi
Shandong Institute of Technology
255012 Zibo, P.R. China

Peter Dietz
Institut für Maschinenwessen, TU-Clausthal,
Robert-Koch-Str. 32, 38678 Clausthal-Zellerfeld, Germany

Xuanli Hu
AUDIAG, I/EG-31, D-85045 Ingolstadt, Germany

(Received August 22, 1997)

This paper presents the expressions of Vibrational Power Flow (VPF) in Beam-Plate Structures (BPS). These expressions are derived based on structural dynamics. BPS is composed of a constant cross-section beam and a thin flat rectangular plate. In expressions the plate is four-edge simply suppored and four-edge fixedly supported, respectively. The numerical calculation of these expressions is implemented. Meanwhile, the different parameters of beam and plate are also considered in the calculation. Finally, the numerical solutions of VPF in BPS are compared with the corresponding the measured VPF. The numerical VPFs have a good agreement with the measured VPF. The results of VPF provide a tool for analyzing vibrational energy transmission between the support roller and the armored plate of tracked vehicles.

Key Words: Vibrational Power Flow (VPF), Mechanical Mobilities and Beam-Plate Structures (BPS).

1. Introduction

BPS are widely applied to vehicular structures or other engineering structures. In BPS when the beam subjects to a harmonic force or an alternative bending moment at its free end, the partial vibrational energy will transfer to the plate which couples with another end of the beam. As the support roller shown in Fig. 1(a), its axle is welded on the side armored plate of tracked vehicles. When the support roller subjects to an external excitation, vibrational energy is easy to transmit to the plate through the axle. It is seen that the axle and the armored plate consist of a typical BPS. The research results in reference [1] indicate that the sound radiation of armored plates relies mostly upon the vibrational energy which is injected through the axle of support rollers.

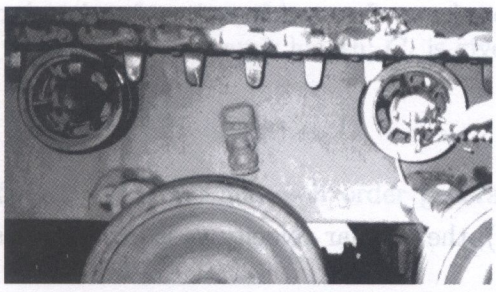

[Fig. 1(a)]

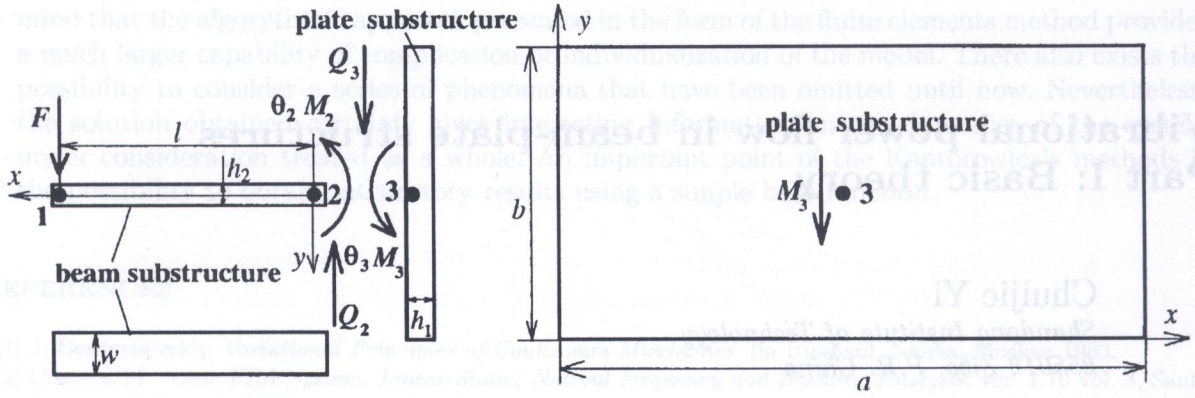

Fig. 1. (a) Support roller; (b) substructures of BPS

The sound radiation of the armored plates is the main noise source inside tracked vehicles [1]. The energy on which the sound radiation depends is mostly transmitted by the axle of support rollers. The key to the noise problem of tracked vehicles is to investigate that the motion behavior of vibrational energy between the roller and the plate; to understand how the parameters of BPS exert an influence on VPF? It is expected that the work be able to lay down a fundation for solving noise problem of tracked vehicles.

2. Expressions of VPF in BPS

As shown in Fig. 1(b), when force F applies at point 1 at the free end of the beam ($x = l$), bending moment M_2 and shear force Q_2 will occur at the joint 2 which is at $x = 0$ on the beam. The angular displacement θ is the relative motion between the beam and the plate. Because a thin flat plate is considered in the analysis, we can neglect the influence of shear force and inertial moment in the plate on plate's vibrational behavior. The BPS in Fig. 1(b) can be divided into a beam substructure and a plate substructure. In the following analysis, only a four-edge simply supported plate is involved. The velocity at point 1 on the beam is given by [2].

$$V_1 = FG_{11} + M_2G_{12} \tag{1}$$

in which G_{11} and G_{12} are the input mobility at point 1 and the transfer mobility between point 1 and 2, respectively. They are defined as

$$G_{ii} = V_i/F_i, \tag{2}$$

$$G_{ij} = V_i/F_j, \tag{3}$$

where V_i is the velocity response at point i; F_i and F_j are respectively the forces at point i and point j. For the moments, the angular displacement and velocity in Fig. 1(b), there are the following equalities.

$$\begin{cases} M_3 = -M_2, \\ \theta_2 = \theta_3, \\ \dot{\theta}_2 = \dot{\theta}_3. \end{cases} \tag{4}$$

In a similar way to Eq. (1), the angular velocity $\dot{\theta}_2$ is expressed as

$$\dot{\theta}_2 = M_2G_{22} + FG_{21}. \tag{5}$$

Combining Eq. (4) with Eq. (5) and considering

$$\theta_3 = M_3 G_{33}, \tag{6}$$

moment M_2 is given by

$$M_2 = -FG_{21}/(G_{22} + G_{33}). \tag{7}$$

Subsituting Eq. (7) into Eq. (1), the input mobility at point 1 is given by

$$G = V_1/F = G_{11} - [G_{12}G_{21}/(G_{22} + G_{33})]. \tag{8}$$

The VPF in the structure including two substructures is defined as [3]

$$P_{\text{in(tr)}} = \frac{1}{2}|F(M)|^2 \text{Re}\left\{G_{i(ij)}\right\}, \tag{9}$$

in which $P_{\text{in(tr)}}$ is the input (transfer) VPF; $F(M)$ is force (moment) and $G_{i(ij)}$ is input (transfer) mobility. Subsituting Eq. (8) into Eq. (9), the input VPF injecting into beam is expressed as

$$P_{\text{in}} = \frac{1}{2}|F|^2 \text{Re}\left\{G_{i(ij)}\right\} = \frac{1}{2}|F|^2 \text{Re}\left\{G_{11} - [G_{12}G_{21}/(G_{22} + G_{33})]\right\}. \tag{10}$$

Substituting Eq. (7) into Eq. (4), moment M_3 is given by

$$M_3 = FG_{21}/(G_{22} + G_{33}). \tag{11}$$

Substituting Eq. (11) into Eq. (9), the transfer VPF from the beam to the plate is expressed as

$$P_{\text{tr}} = \frac{1}{2}|M_3|^2 \text{Re}\{G_{33}\} = \frac{1}{2}|F|^2 |G_{21}/(G_{22} + G_{33})|^2 \text{Re}\{G_{33}\}. \tag{12}$$

Evidently, in order to know VPF in BPS, the first step is to get the input and transfer mobilities related to the beam and the plate.

3. Mobilities related to beam

The general form of vibrational equation of beam yields [4]

$$E^* I \frac{\partial^4 y}{\partial x^4} + \rho A_b \frac{\partial^2 y}{\partial t^2} = p(x,t) - \frac{\partial}{\partial x} m(x,t), \tag{13}$$

where $E^* = E(1 + i\eta)$ is the complex modules of elasticity and η the structural loss factor; I the inertial moment; ρ the material density and A_b the cross-section area of beam. For distributed force $p(x,t)$ the solution of Eq. (13) may be supposed to be

$$y(x,t) = \sum_{j=1}^{\infty} C_j Y_j(x) e^{i\omega t}, \tag{14a}$$

in which $Y_j(x)$ is the j-th order eigenfunction of beam. It can be expressed as $Y_j(x) = \text{sh}\beta_j x + r_j \sin\beta_j x$, where $r_j = \text{sh}\beta_j l / \sin\beta_j l$; l is the beam's length; C_j is given by

$$C_j = P_j / \left\{M_j \left[\omega_j^2(1 + i\eta) - \omega^2\right]\right\}, \tag{14b}$$

where $P_j = \int_0^l F_0 \sigma(x - l) Y_j(x) dx = F_0 Y_j(l)$ and j-th order generalized mass of beam is $M_j = \int_0^l \rho A Y_j^2(x) dx$.

3.1. Input mobility G_{11} and transfer mobility G_{21}

Substituting Eq. (14a) into Eq. (13) and then taking force $p(x,t)$ in Eq. (13) as a simple harmonic force $F_0 e^{i\omega t}$, Eq. (14a) is simplified by

$$y(x,t) = \sum_{j=1}^{\infty} F_0 Y_j(l) Y_j(x) e^{i\omega t} / \left\{ M_j \left[\omega_j^2 (1 + i\eta) - \omega^2 \right] \right\}. \tag{15}$$

By differentiation with respect to time t of Eq. (15), the velocity at point 1 on the beam is given by

$$V_1 = \partial y(x,t)/\partial t \,|_{x=l} = \sum_{j=1}^{\infty} F_0 Y_j^2(l) e^{i\omega t}(i\omega) / \left\{ M_j \left[\omega_j^2 (1 + i\eta) - \omega^2 \right] \right\}. \tag{16}$$

In term of Eq. (2) input mobility G_{11} is expressed as

$$G_{11} = \sum_{j=1}^{\infty} Y_j^2(l)\omega / \left\{ M_j \omega_j^2 \left[\eta + i(\lambda_j - 1) \right] \right\}, \tag{17}$$

where λ_j is frequency rate, i.e., $\lambda_j = \omega^2/\omega_j^2$. Differentiating with respect to x and t of Eq. (15), angular velocity at point 2 on the beam is given by

$$\dot{\theta}_2 = \partial^2 y(x,t)/\partial x \partial t \,\Big|_{x=0} = \sum_{j=1}^{\infty} Y_j(l) Y_j(0) F_0 e^{j\omega t}(i\omega) / \left\{ M_j \left[\omega_j^2 (1 + i\eta) - \omega^2 \right] \right\}. \tag{18}$$

And then by means of Eq. (3), the transfer mobility between point 1 and point 2 on the beam yields

$$G_{21} = \sum_{j=1}^{\infty} Y_j(0) Y_j(l)\omega / \left\{ M_j \omega_j^2 \left[\eta + i(\lambda_j - 1) \right] \right\}. \tag{19}$$

3.2. Input mobility G_{22} and transfer mobility G_{12}

When a moment excitation presents the harmonic form, i.e., $m(x,t) = -M_0 e^{j\omega t}\delta(x-0)$, Eq. (14a) is also expressed as

$$y(x,t) = \sum_{j=1}^{\infty} -Y_j'(0) Y_j(x) M_0 e^{i\omega t} / \left\{ M_j \left[\omega_j^2 (1 + i\eta) - \omega^2 \right] \right\}. \tag{20}$$

The velocity at point 1 and the angular velocity at 2 point on the beam are given by, respectively

$$V_1 = \partial y(x,t)/\partial t \,|_{x=l} = \sum_{j=1}^{\infty} -Y_j'(0) Y_j(l) M_0 e^{i\omega t}(i\omega) / \left\{ M_j \left[\omega_j^2 (1 + i\eta) - \omega^2 \right] \right\}, \tag{21}$$

$$\dot{\theta_2} = \partial^2 y(x,t)/\partial x \partial t \,|_{x=l} = \sum_{j=1}^{\infty} -\left[Y_j'(0) \right]^2 M_0 e^{i\omega t}(i\omega) / \left\{ M_j \left[\omega_j^2 (1 + i\eta) - \omega^2 \right] \right\}. \tag{22}$$

Substituting respectively Eq. (22) into Eq. (2) and Eq. (21) into Eq. (3), G_{22} and G_{12} are given by

$$G_{22} = \sum_{j=1}^{\infty} \left[Y_j'(0) \right]^2 \omega / \left\{ M_j \omega_j^2 \left[\eta + i(\lambda_j - 1) \right] \right\}, \tag{23}$$

$$G_{12} = \sum_{j=1}^{\infty} Y_j'(0) Y_j(l)\omega / \left\{ M_j \omega_j^2 \left[\eta + i(\lambda_j - 1) \right] \right\}. \tag{24}$$

4. INPUT MOBILITY RELATED TO PLATE

4.1. Input mobility of four-edge simply supported plates

The vibration equation of thin plates yields [5]

$$B\nabla^2\nabla^2 w(1+i\eta)+\rho A_p\frac{\partial^2 w}{\partial t^2}=q(x,y,t), \tag{25}$$

where $B=Eh^3/[12(1-\mu^2)]$ is the complex stiffness of plates in which E is the modules of elasticity, h the thickness and μ Poisson's ratio; ρ the plate's density; η the plate's loss factor; A_p, the area of the plate and $q(x,y,t)$ the load per unit area of the plate. The closed solution of Eq. (25) is given by

$$w(x,y,t)=\sum_{m=1}^{\infty}\sum_{n=1}^{\infty}\frac{4n\pi\sin(m\pi x_0/a)\cos(n\pi y_0/b)\sin(m\pi x/a)\sin(n\pi y/b)}{ab^2\rho h\left[\omega_{m,n}^2(1+i\eta)-\omega^2\right]}M_0e^{i\omega t}. \tag{26}$$

Based on the equation above, the angular velocity at point 3 on plate in direction y is given by

$$\dot\theta_y(x_0,y_0)=\left.\frac{\partial^2 w(x,y,t)}{\partial y\partial t}\right|_{x=x_0,y=y_0}=\sum_{m=1}^{\infty}\sum_{n=1}^{\infty}\frac{4n^2\pi^2(i\omega)\sin^2\left(\dfrac{m\pi x_0}{a}\right)\cos^2\left(\dfrac{n\pi y_0}{b}\right)}{ab^3\rho h\left[\omega_{m,n}^2(1+i\eta)-\omega^2\right]}M_0e^{i\omega t} \tag{27}$$

Substituting Eq. (27) into Eq. (2), the input mobility of plate yields

$$G_{33}=\frac{\dot\theta_y(x_0,y_0)}{M_3}=\sum_{m=1}^{\infty}\sum_{n=1}^{\infty}\sin^2(m\pi x_0/a)\cos^2(n\pi y_0/b))\frac{4\omega n^2\pi^2}{ab^3\rho h\omega_{m,n}^2\left[\eta+i(\lambda_{m,n}-1)\right]}. \tag{28}$$

4.2. Input mobility of four-edge fixedly supported plates

The response of fixedly supported plates can be supposed to be the folowing form

$$w(x,y,t)=\sum_{m=1}^{\infty}\sum_{n=1}^{\infty}W_{m,n}(x,y)C_{m,n}e^{i\omega t}, \tag{29}$$

where $W_{m,n}(x,y)$ is the (m,n)-th orders eigenfunction; $C_{m,n}=(P_{m,n}/M_{m,n})\left[\omega_{m,n}^2(1+i\eta)-\omega^2\right]$ in which $P_{m,n}=M_0\partial W_{m,n}(x_0,y_0)/\partial y$ and $M_{m,n}=\int\int_s\rho hW_{m,n}^2(x,y)ds$ which is (m,n)-th orders generalized mass of plate. Refer to [5], the approximate solution of eigenfunction $W(x,y)$ in Eq. (29) yields

$$W(x,y)=\sum_{m=1}^{\infty}\sum_{n=1}^{\infty}C_{m,n}X_m(x,)Y_n(y), \tag{30}$$

where

$$\begin{aligned}
X_m(x) &= (\cos\beta_m x-\mathrm{ch}\beta_m x)+r_m(\sin\beta_m x-\mathrm{sh}\beta_m x),\\
Y_n(y) &= (\cos\alpha_n y-\mathrm{ch}\alpha_n y)+s_n(\sin\alpha_n y-\mathrm{sh}\alpha_n y),\\
\beta_m &= \frac{[m+(1/2)]\,\pi}{a};\quad r_m=(\cos\beta_m a-\mathrm{ch}\beta_m a)/(\sin\beta_m a-\mathrm{sh}\beta_m a),\\
\alpha_n &= \frac{[n+(1/2)\pi}{b};\quad s_n=(\cos\alpha_n b-\mathrm{ch}\alpha_n b)/(\sin\alpha_n b-\mathrm{sh}\alpha_n b).
\end{aligned}$$

Substituting Eq. (29) into Eq. (2), the input mobility at point 3 of four-edge fixedly supported plates yields

$$G_{33} = \sum_{m=1}^{\infty}\sum_{n=1}^{\infty}\left[\frac{\partial W_{m,n}(x_0,y_0)}{\partial y}\right]^2 \frac{\omega}{\omega_{m,n}^2\left[\eta + i(\lambda_{m,n}-1)\right]\int\int_s \rho h W_{m,n}^2(x,y)ds}. \tag{31}$$

5. VPF EXPRESSIONS OF BPS

5.1. VPF Expressions of BPS in the case of four-edge simply supported plates

Substituting in turn Eqs. (17), (19), (23), (24) and (28) into Eq. (10), and then Eqs. (19), (23) and (28) into Eq. (12), the input and transfer VPSs in BPS are given by

$$P_{\text{in}} = \frac{1}{2}|F|^2\,\text{Re}\left\{\sum_{m=1}^{\infty}\frac{Y_m^2(l)\omega}{M_m\omega_m^2[\eta - i(1-\lambda_m)]}\left\{1 - ab^3\rho h[Y_m'(0)]^2\sum_{n=1}^{\infty}\right.\right.$$

$$\left.\left.\frac{(\omega_{m,n}^2-\omega^2)}{ab^3\rho h[Y_m'(0)]^2(\omega_{m,n}^2-\omega^2) + M_m\omega_m^2[\eta - i(1-\lambda_m)]\times\left[4\omega n^2\pi^2\sin^2\left(\frac{m\pi x_0}{a}\right)\cos^2\left(\frac{n\pi y_0}{b}\right)\right]}\right\}\right\}, \tag{32}$$

$$P_{\text{tr}} = \frac{1}{2}|F|^2\sum_{m=1}^{\infty}\sum_{n=1}^{\infty}$$

$$\left\{\left|\frac{ab^3\rho h Y_m'(0)Y_m'(l)(\omega_{m,n}^2-\omega^2)}{ab^3\rho h[Y_m'(0)]^2(\omega_{m,n}^2-\omega^2) + \left[4n^2\pi^2\omega\omega_m^2[\eta - i(1-\lambda_m)]\sin^2\left(\frac{m\pi x_0}{a}\right)\cos^2\left(\frac{n\pi y_0}{b}\right)\right]}\right|^2\right.$$

$$\left.\times\left\{\frac{4n^2\pi^2\omega(\omega_{m,n}^2-\omega^2)\sin^2\left(\frac{m\pi x_0}{a}\right)\cos^2\left(\frac{n\pi y_0}{b}\right)}{ab^3\rho h\left[(\omega_{m,n}^2-\omega^2)+\omega_{m,n}^2\eta^2\right]}\right\}\right\}. \tag{33}$$

5.2. VPF Expressions of BPS in the case of four-edge fixedly supported plates

In Eqs. (10) and (12) only substituting the input mobility of four-edge fixedly supported plate for the input mobility of four-edge simply supported plate, the expressions of input and transfer VPFs are given by

$$P_{\text{in}} = \frac{1}{2}|F|^2\left\{\sum_{m=1}^{\infty}\frac{[Y_m(l)]^2\omega}{M_m\omega_m^2[\eta - i(1-\lambda_m)]}\right\}\left\{1 - \sum_{m=1}^{\infty}\frac{[Y_m'(0)]^2}{\Lambda(m,n)}\right\}, \tag{34}$$

where

$$\Lambda(m,n) = M_m\omega_m^2[\eta - i(1-\lambda_m)]\left\{\frac{\omega[Y_m'(0)]^2}{M_m\omega_m^2[\eta - i(1-\lambda_m)]} + \left[\frac{\partial W_{m,n}(x_0,y_0)}{\partial y}\right]^2\right.$$

$$\left.\left\{\frac{\omega}{\rho h(\omega_{m,n}^2-\omega^2)\int\int_s W_{m,n}^2(x,y)dxdy}\right\}\right\},$$

$$P_{\mathrm{tr}} = \frac{1}{2}|F|^2 \sum_{m=1}^{\infty}\sum_{n=1}^{\infty}\left|\frac{Y'_m(0)Y'_m(l)}{\Psi(m,n)}\right|^2 \left\{\frac{\omega^3(\lambda_m^2-1)\left[\dfrac{\partial W_{m,n}(x_0,y_0)}{\partial y}\right]^2}{\rho h\left[(\omega_{m,n}^2-\omega^2)^2+(\omega_{m,n}^2\eta)^2\displaystyle\int\!\!\int_s W_{m,n}^2(x,y)dxdy\right]}\right\}, \quad (35)$$

in which

$$\Psi(m,n) = \omega[Y'_m(0)]^2 + \left\{\rho h M_m\omega_{m,n}^2(\omega_m^2-\omega^2)[\eta - i(1-\lambda_m)]\left[\frac{\partial W_{m,n}(x_0,y_0)}{\partial y}\right]^2\int\!\!\int_s W_{m,n}^2(x,y)dxdy\right\}.$$

6. NUMERICAL SOLUTIONS OF VPF IN BPS

The numerical solutions of Eqs. (32)–(35) are represented in Figs. 2 through 7. In these numerical solutions, the sizes of beam are $l = 300$ mm (length), $w = 50$ mm (width) and $h_2 = 5$ mm (thickness); the sizes of plate are $a = 1000$ mm (length), $b = 500$ mm (width) and $h_1 = 6$ mm (thickness). The beam and plate are tha same material, i.e., carbon steel. Its elasticity E, Poisson ratio μ and density ρ are 2.0×10^{11} N/m^2, 0.03 and 7800 kg/m^2, respectively. The frequency range of the numerical calculation of VPF is from 0 Hz to 1000 Hz.

Under the boundary conditions of four-edge simply supported and fixedly supported plates, in the following numerical VPF, it is involved that the different thicknesses and areas of plates, the different lengths of beams, the different coupling positions between beam and plate and the different loss factor rates of beams to plates.

6.1. Different thickness and areas of plates

When the size of beam is unchangeable, and only the thicknesses of plates are taken as 3 mm, 6 mm and 15 mm, the numerical solutions are shown in Fig. 2 and Fig. 3. The average VPF in analytical frequency range are listed in Table 1. In Fig. 2(b) the sizes of beam and plate are $300 \times 50 \times 5$ mm and $1000 \times 500 \times 6$ mm, respectively.

Table 1. Average VPF in BPS in the cases of different thicknesses and areas of plates

thicknesses $(h_1)^*$	3 mm	6 mm	15 mm	areas $(a \times b)^*$	0.23 m^2	0.5 m^2	1.13 m^2
$\overline{P}_{\mathrm{in}}(dB)$	−2.17	−2.18	−2.19	$\overline{P}_{\mathrm{in}}(dB)$	−2.20	−2.18	−2.15
$\overline{P}_{\mathrm{tr}}(dB)$	−2.97	−3.27	−4.30	$\overline{P}_{\mathrm{tr}}(dB)$	−4.15	−3.27	−3.21

Note: * other parameters of the plate and the beam are the same as the parameters of the beam and the plate in Fig. 2(b).

According to the results represented in Fig. 2, Fig. 3 and Table 1, it is clear that (1) the thickness of the plate has greater influence on the transfer VPF than on the input VPF; (2) when increasing plate's thickness, the transfer VPF will be much less than the input VPF. If plate's thickness increasing by 3 mm, i.e., the thickness from 3 mm to 6 mm, the transfer VPF will only decrease by 0.3 dB. However, when increasing plate's thickness by 9 mm i.e., thickness from 6 mm to 15 mm, the transfer VPF will decreased by 1.03 dB. This is why input mobility G_{33} in Eq. (28) will decrease with the increase of plate's thickness. The plate's input mobility G_{33} has relative strong ability to

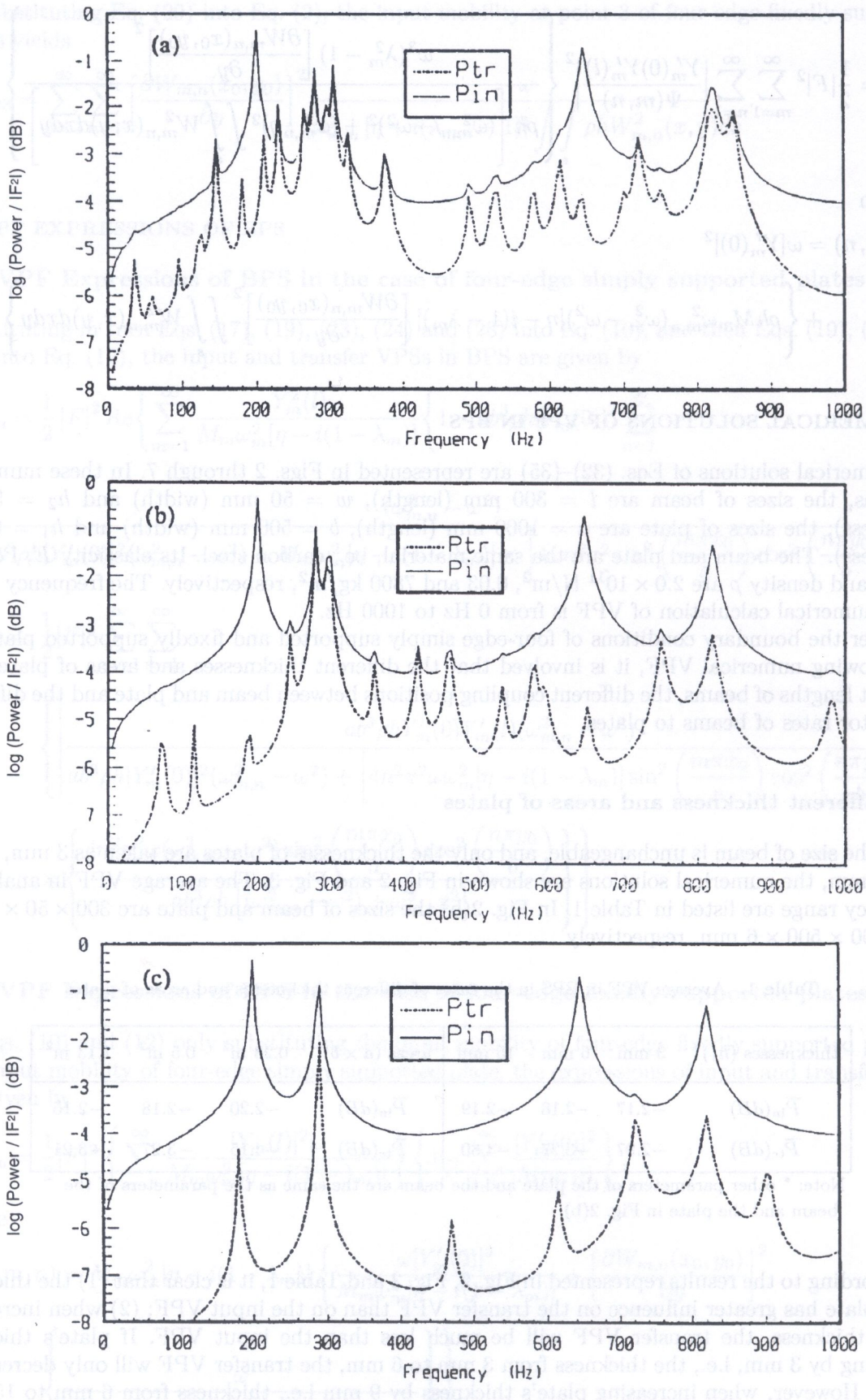

Fig. 2. VPF in BPS in the cases of different thicknesses of plates; (a) $h_1 = 3$ mm ($a \times b = 0.5$ m^2); (b) $h_1 = 6$ mm($a \times b = 0.5$ m^2); (c) $h_1 = 15$ mm($a \times b = 0.5$ m^2); beam: ($l \times w \times h_2 = 300 \times 50 \times 5$ mm); – input VPF; ... transfer VPF

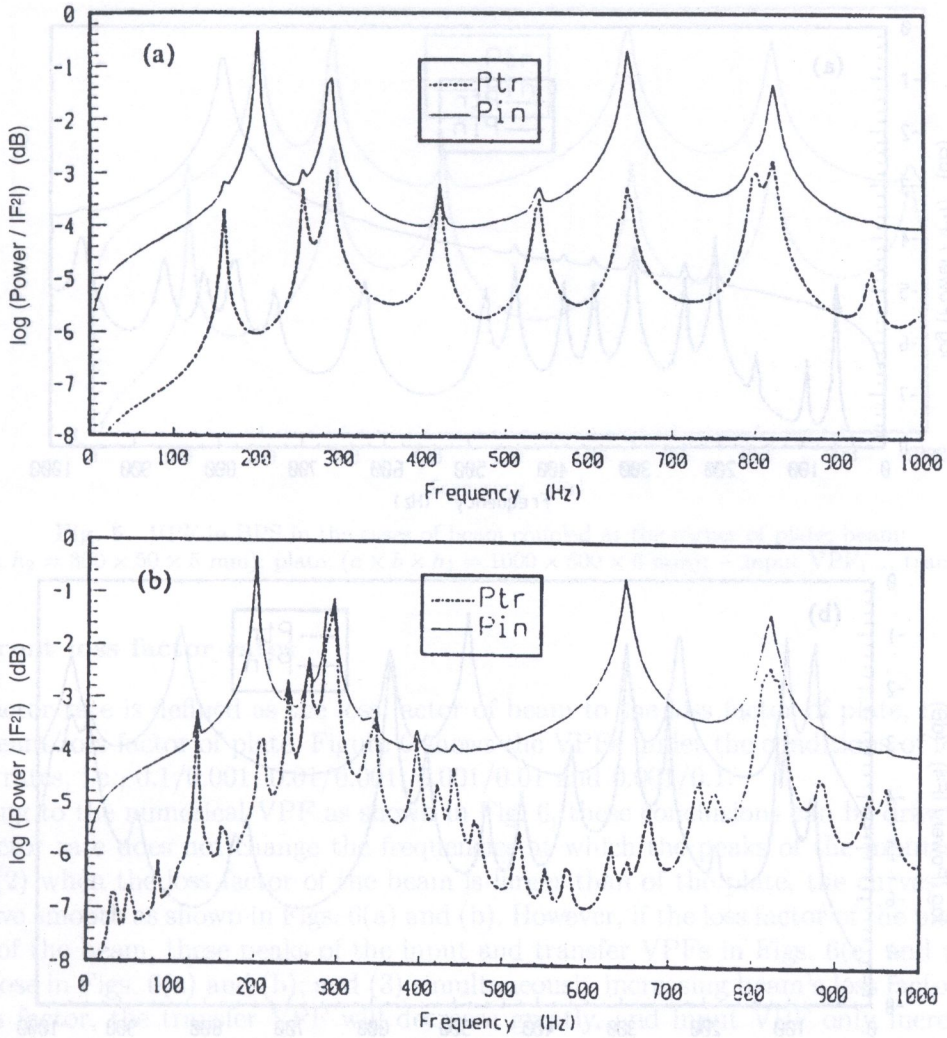

Fig. 3. VPF in BPS in the cases of different areas of plates; (a) $a \times b = 0.23$ m^2($h_1 = 6$ mm); (b) $a \times b = 1.13$ m^2($h_1 = 6$ mm); beam: ($l \times w \times h_2 = 300 \times 50 \times 5$ mm); – input VPF; ... transfer VPF

govern the transfer VPF; and (3) because natural frequencies of plate decrease with the increase its area, increasing plate's area will result in much plate's more modes to participate in VPF. Consequently, both input and transfer VPFs will increase. When increasing plate's area by 0.27 m^2 (the area from 0.23 m^2 to 0.5 m^2), the transfer VPF will be increased by 0.88 dB. But if increasing the area by 0.613 m^2 (the area from 0.5 m^2 to 1.13 m^2), the transfer VPF is only increased by 0.06 dB. Evidently, when plates area is relative small, it is more easy for VPF to transmit from the beam to the plate.

6.2. Different lengths of beams

For three different length beams, i.e., 150 mm, 300 mm and 500 mm, the numerical solutions of VPF are shown in Fig. 4. When beam is 300 mm long, the calculated results are the same as those shown in Fig. 2(b).

Figure 4 shows that (1) even though the input and transfer VPFs all increase with the increase of beam's length, the influence of beam's length on input VPF is not great as on transfer VPF; (2) when increasing beam's length by 150 mm, i.e., the length 150 mm to 300 mm, the transfer VPF will be increased by 1.97 dB. However, the length is increased by 300 mm (from 300 mm to

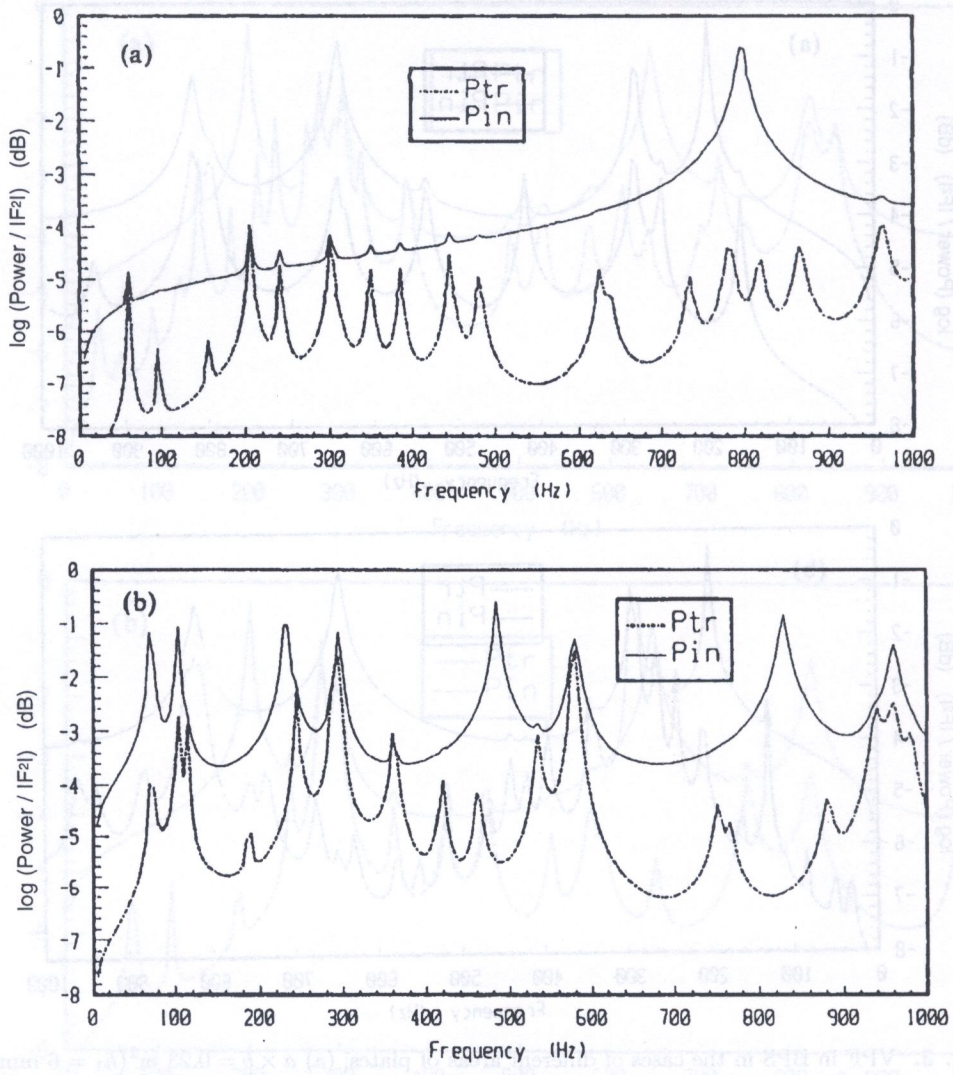

Fig. 4. VPF in BPS in the cases different lengths of beams; (a) $l = 150$ mm ($h_2 = 5$ mm, $w = 50$ mm); (b) $l = 500$ mm ($h_2 = 5$ mm, $w = 50$ mm); plate: ($a \times b \times h_1 = 1000 \times 500 \times 6$ mm); – input VPF; ... transfer VPF

500 mm), the transfer VPF do almost not increase. Thus the plate which couples with a relative short beam is to absorb VPF easily; and (3) as shown in Fig. 4, for the relative long beam the peak amplitudes of the input VPF will increase.

6.3. Different coupling positions between the beam and the plate

Figure 5 shows the numerical VPF in the case of the beam coupling at plate's corner. When the beam couples with plate's center, the numerical VPF have been given in Fig. 2(b) before.

Comparing Fig. 5 with Fig. 2(b), the input VPF in the case of the beam coupled at the corner of the plate is 0.68 dB greater than coupled at the center of the plate. For transfer VPF, on the contrary, the former is less than the latter by 0.73 dB. This is the reason that the input mobility of late's center is greater than that at plate's corner. In addition, when a corner of plate subjects to an excitation, there will be much more plate's modes to participate in VPF. Hence for this case the transfer VPF will increase greatly.

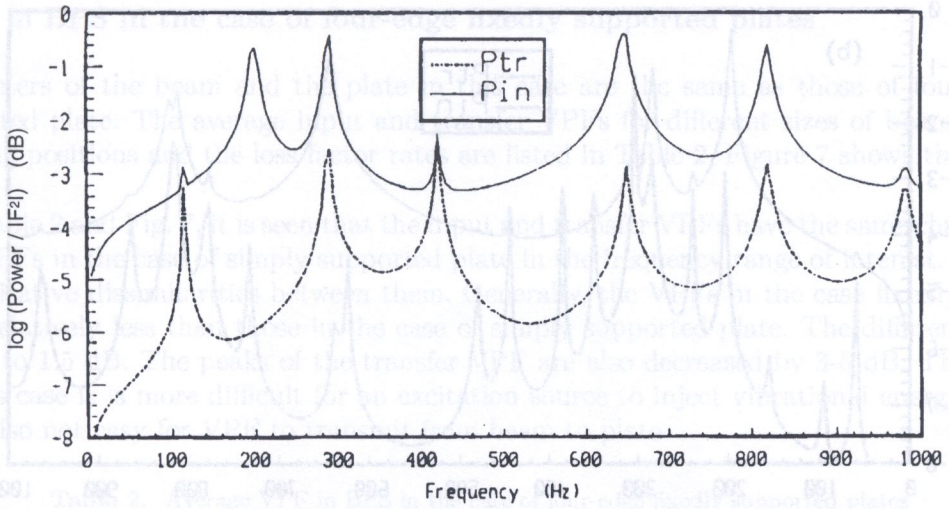

Fig. 5. VPF in BPS in the cases of beam coupled at the corner of plate; beam: $(l \times w \times h_2 = 300 \times 50 \times 5$ mm); plate: $(a \times b \times h_1 = 1000 \times 500 \times 6$ mm); – input VPF; ... transfer VPF

6.4. Different loss factor rates

The loss factor rate is defined as the loss factor of beam to the loss factor of plate, i.e., R_d = loss factor of beam/loss factor of plate. Figure 6 shows the VPFs under the conditions of four different loss factor rates, i.e., 0.1/0.001, 0.01/0.001, 0.001/0.01 and 0.001/0.1.

According to the numerical VPF as shown in Fig. 6, these conclusions can be drawn below. (1) the loss factor rate does not change the frequencies at which the peaks of the input and transfer VPF are; (2) when the loss factor of the beam is larger than of the plate, the curves of the input VPF relative smooth as shown in Figs. 6(a) and (b). However, if the loss factor of the plate is greater than that of the beam, these peaks of the input and transfer VPFs in Figs. 6(c) and (d) is not so steep as those in Figs. 6(a) and (b); and (3) simultaneously increasing beam's loss factor decreasing plate's loss factor, the transfer VPF will decrease greatly, and input VPF only increase slightly. When beam's loss factor is far greater than plate's loss factor by about two-order of magnitudes, the transfer VPF is 2.35 dB less than the input VPF. In other words, the transfer VPF is less than 5 thousandths of the input VPF.

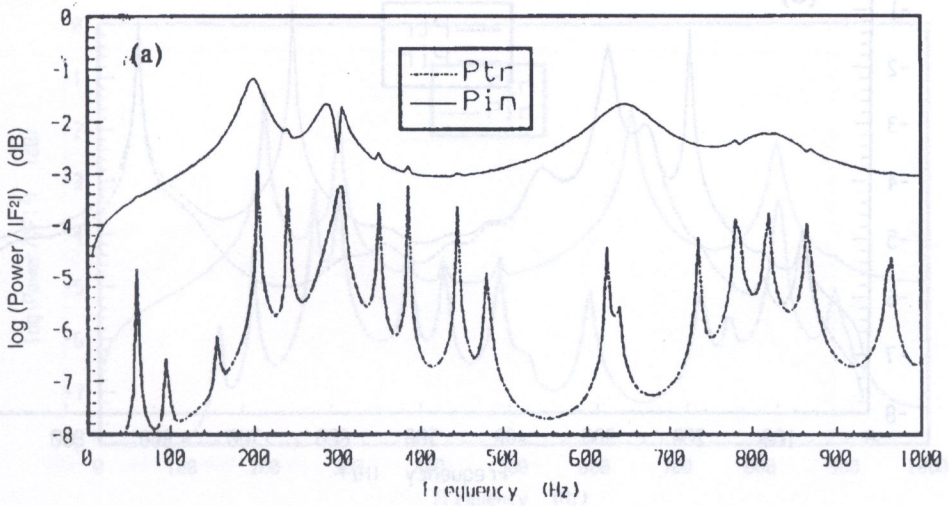

[Fig. 6(a)]

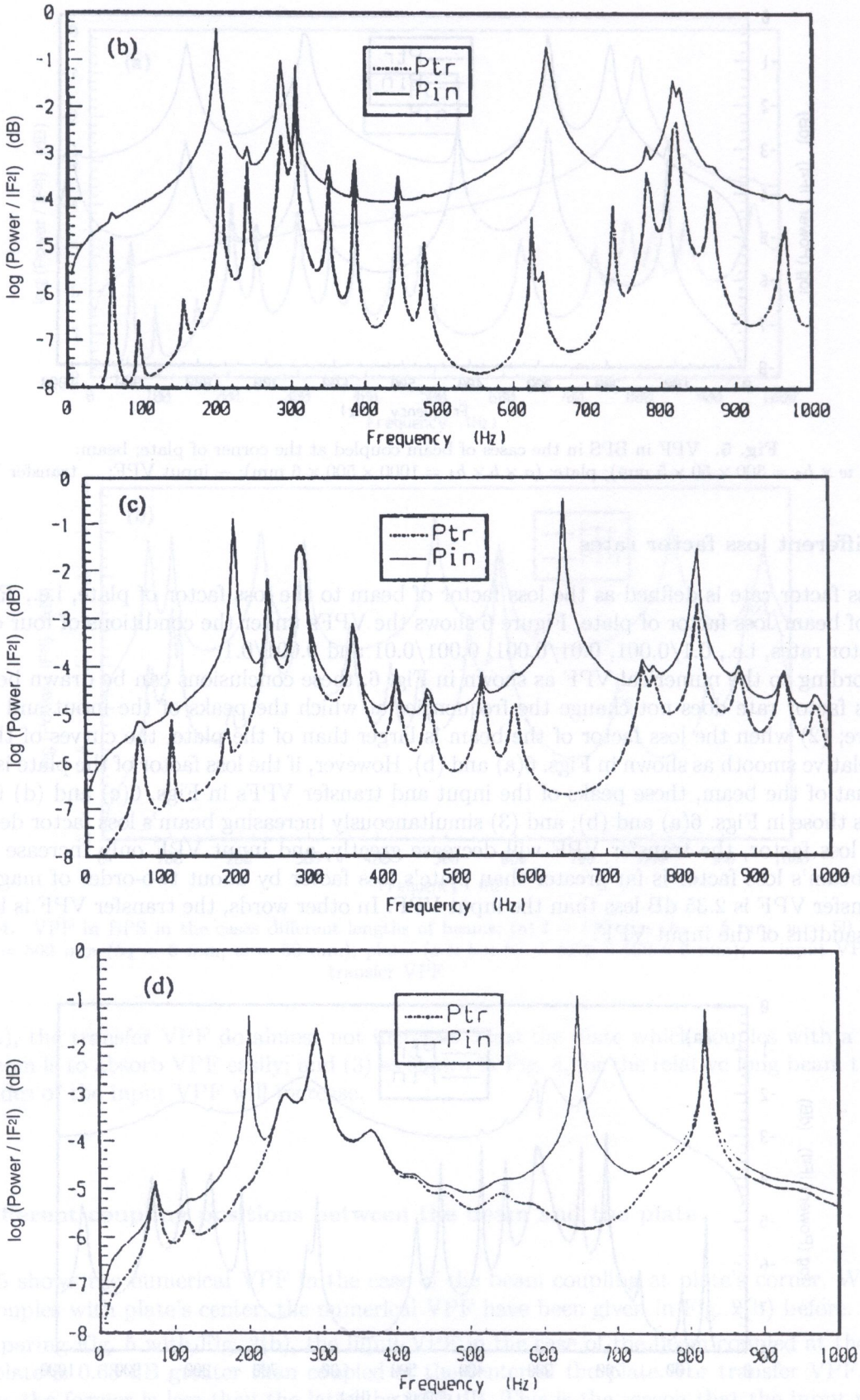

Fig. 6. VPF in BPS in the cases of different loss factor rates; (a) 0.1/0.001; (b) 0.01/0.001; (c) 0.001/0.01 and (d) 0.001/0.1; beam: ($l \times w \times h_2 = 300 \times 50 \times 5$ mm); plate ($a \times b \times h_1 = 1000 \times 500 \times 6$ mm); – input VPF; ... transfer VPF

6.5. VPF in BPS in the case of four-edge fixedly supported plates

All parameters of the beam and the plate in this case are the same as those of four-edge simply supported plate. The average input and transfer VPFs for different sizes of beams or plates, the coupling positions and the loss factor rates are listed in Table 2. Figure 7 shows the numerical VPF.

From Table 2 and Fig. 7, it is seen that the input and transfer VPFs have the same characteristics as those VPFs in the case of simply supported plate in the frequency range of interest. There exist only quantitative dissimilarities between them. Generally, the VPFs in the case fixedly supported plate are relatively less than those in the case of simply supported plate. The difference is about from 1 dB to 1.5 dB. The peaks of the transfer VPF are also decreased by 3-5 dB. This indicates that in this case it is more difficult for an excitation source to inject vibrational energy into BPS. And it is also not easy for VPF to transmit from beam to plate.

Table 2. Average VPF in BPS in the case of four-edge fixedly supported plates

Plate thicknesses*	3 mm	6 mm	15 mm	Plate areas*	0.23 m^2	0.5 m^2	1.13 m^2
$\overline{P}_{in}$ (dB)	−3.06	−3.08	−3.09	$\overline{P}_{in}$ (dB)	−3.09	−3.08	−3.07
$\overline{P}_{tr}$ (dB)	−4.09	−4.80	−6.30	$\overline{P}_{tr}$ (dB)	−5.68	−4.80	−4.05
Beam lengths*	150 mm	300 mm	500 mm	Coupling positions*	Center	Corner	
$\overline{P}_{in}$ (dB)	−3.37	−3.08	−3.04	$\overline{P}_{in}$ (dB)	−2.32	−3.08	
$\overline{P}_{tr}$ (dB)	−6.55	−4.80	−4.74	$\overline{P}_{tr}$ (dB)	−5.28	−4.80	
Loss factor rates*	0.1/0.001			0.01/0.001	0.0001/0.01	0.001/0.1	
$\overline{P}_{tr}$ (dB)	−3.15			−3.07	−3.30	−3.40	
$\overline{P}_{tr}$ (dB)	−5.90			−5.07	−4.20	−3.86	

Note: * other parameters are the same as those of the BPS in Fig. 2(b).

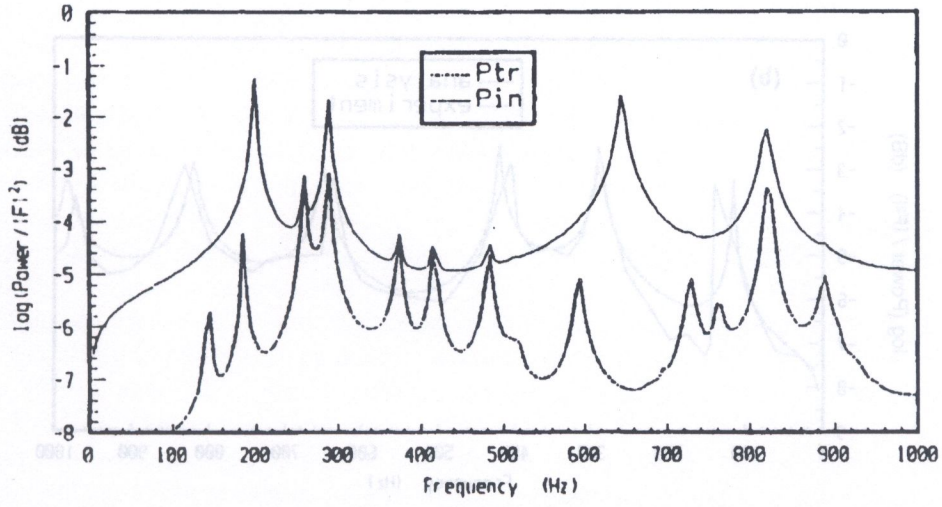

Fig. 7. VPF in BPS in the cases of four-edge fixedly supported plates; beam: $(l \times w \times h_2 = 300 \times 50 \times 5$ mm); plate: $(a \times b \times h_1 = 1000 \times 500 \times 6$ mm); – input VPF; ... transfer VPF

7. VPF MEASUREMENT

In the VPF measurement the sizs of beam and the plate are $300 \times 50 \times 5$ mm and $1000 \times 500 \times 6$ mm, respectively. The beam couples in plate's center. Only four-edge supported plate is considered in this measurement. The four edges of the plate and the free end of the beam all are treated by the damping material. And the corresponding measurement devices are shown in Fig. 8 [6]. The input VPF can be adjusted easily by means of the measured device. Comparing the measured VPF with calculated VPF in Fig. 9, it is seen that (1) the measured VPF has an agreement with the calcu-

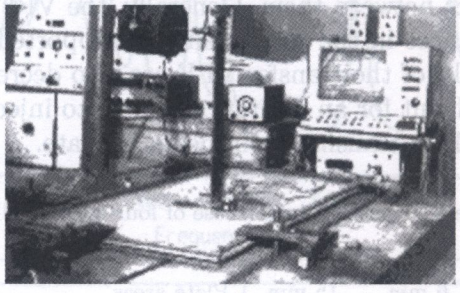

Fig. 8. Measured devices of VPF in BPS; beam: $(l \times w \times h_2 = 300 \times 50 \times 5$ mm); plate: $(a \times b \times h_1 = 1000 \times 500 \times 6$ mm)

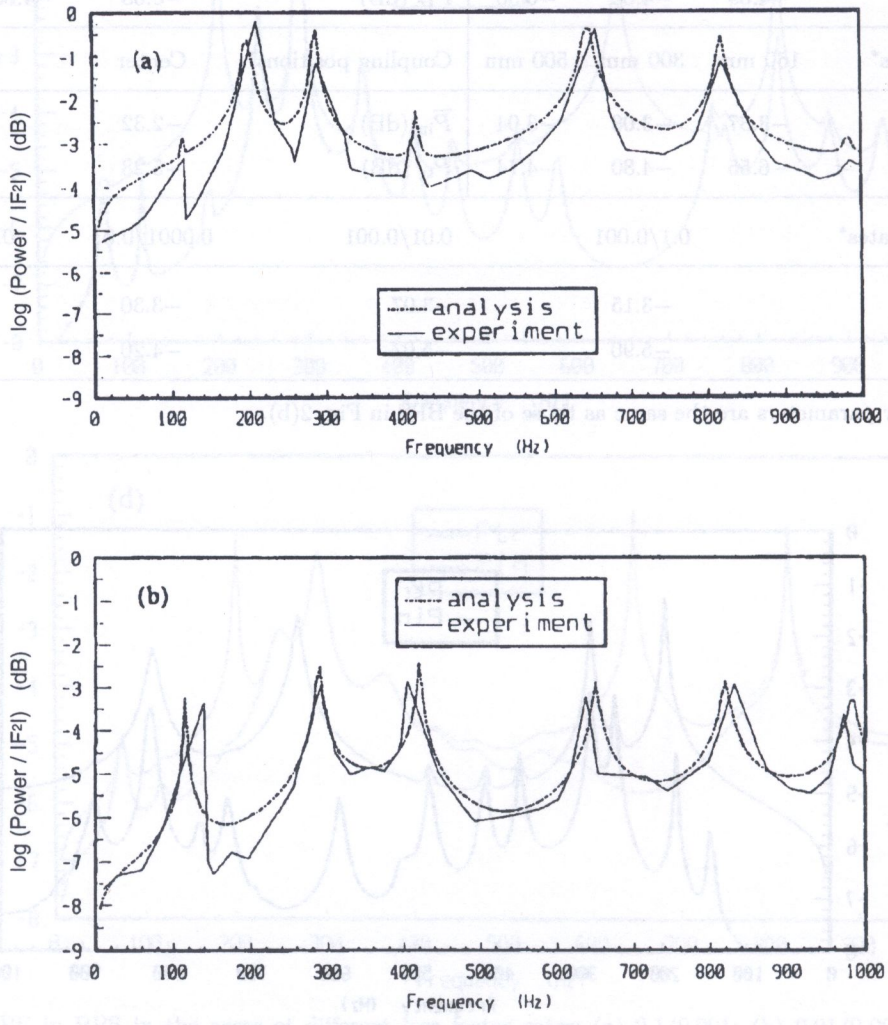

Fig. 9. Measured VPF in BPS (a) input VPF (b) transfer VPF; beam: $(l \times w \times h_2 = 300 \times 50 \times 5$ mm); plate: $(a \times b \times h_1 = 1000 \times 500 \times 6$ mm; – input VPF; ... transfer VPF

lated VPF in the frequency range of interest. The maximum error between them is below 13%; and (2) the error at the frequencies well above 300 Hz is not so large as at frequencies below the frequency.

8. Conclusion

(1) The thickness and area of plate have greater influence on the transfer VPF than on the input VPF. Simultaneously with increasing plate's and thickness decreasing its area, the transfer VPF will be decreased.

(2) The input and transfer VPFs are very sensitive to beam's length change. They will decrease with shorting beam's length.

(3) The transfer VPF in the case of beam coupling at a corner of plate is greater than coupled in the case of beam coupling in plate's center.

(4) Simultaneously with increasing beam's loss factor and decreasing plate's loss factor, i.e., increasing the loss factor rate, the transfer VPF in BPS will be reduced effectively.

These conclusions have been applied to analyzing vibrational energy transmission between the support roller and the armored plate of tracked vehicles mentioned in section 1 before.

References

[1] C. Yi, C. Wu, G. Lu and X. Huang. Techniques of interior noise control in armored personnel carriages, *Acta Armamentarii*, **16**: 73–77, 1995.

[2] H. Zuo. *Analytical Method and Practical Application of Mechanical Impedance*, China Machine Press, 1 st edition, 1987.

[3] C. Yi, T. Chen, H. Huang and W. Li. Power flow in assemlies of connected plates with bean bag damping, *Acta Mechanica* Sinica, **27**:4, 495–500, 1995.

[4] Z. Zheng. *Mechanical Vibration*, China Machine Press, 1st edition, 1989.

[5] Z. Cao. *Vibration Theory of Plate and Shell.* China Railway Press, 1st edition, 1989.

[6] C. Yi, G. Lu and X. Huang. Research of vibrational intensity on complex structures, *Chinese J. of the Applied Mechanics*, **10**: 40–47, 1993.